AIAA 99-0122
A Solution on the F-18C for Store Separation Simulation Using *Cobalt*$_{60}$

R. F. Tomaro, F. C. Witzeman and W. Z. Strang
Computational Sciences Branch
Air Vehicles Directorate
Air Force Research Laboratory
Wright-Patterson AFB, OH

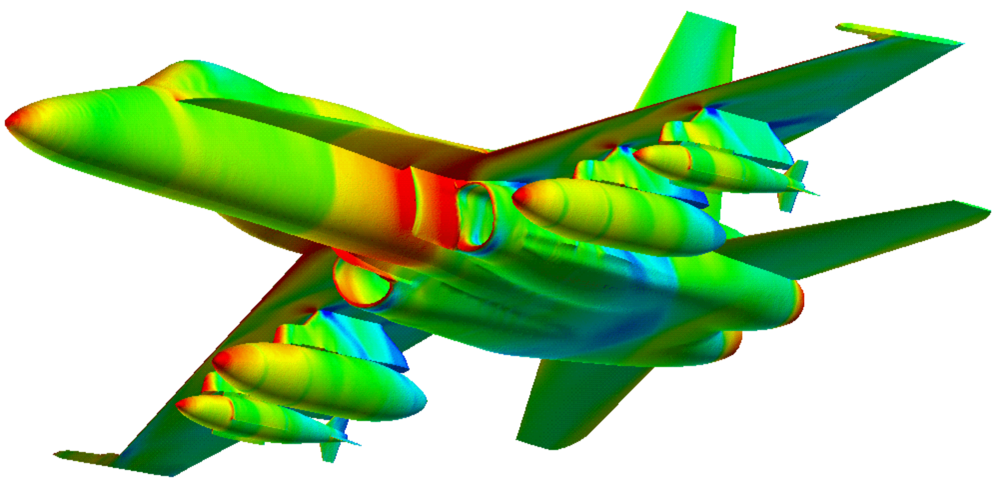

A SOLUTION ON THE F-18C FOR STORE SEPARATION SIMULATION USING *Cobalt*$_{60}$

Robert F. Tomaro*, Frank C. Witzeman* and William Z. Strang*
Air Force Research Laboratory
Air Vehicles Directorate
WPAFB Ohio 45433

Abstract

A demonstration is presented of the ability of Computational Fluid Dynamics (CFD) methods to predict store carriage loads and support store trajectory generation. A complete, complex aircraft, the F/A-18C, was modeled with actual stores in their carriage positions. *Cobalt*$_{60}$, a parallel, implicit unstructured flow solver was used to calculate the flow field and resultant aerodynamic loads on grids composed of tetrahedral cells. Three grids were used to simulate three different flow field approximations. The first grid was a purely inviscid grid containing 3.15 million cells. The second grid was made up of 3.96 million cells clustered to capture viscous effects on only the store components. The third grid was a full viscous grid containing 6.62 million cells. Store carriage loads for two flight conditions were calculated and compared with wind-tunnel measurements and flight-test data for each of the above grids. The resulting carriage loads were used in a separate six degree-of-freedom (6DOF) rigid-body motion code to generate store trajectories. All CFD solutions were second-order accurate and run to steady-state with CFL numbers of one million. Turnaround times ranged from 6 to 21 hours, depending on the number of processors used.

Introduction

The incorporation of CFD tools into the store certification process is limited at the present. Accurate, reliable answers must be provided quickly and economically. First, the entire solution process must be accomplished in a matter of days. With the maturing of the unstructured grid generation process, full viscous grids can be generated in under a week's time on very complex configurations. Using massively parallel supercomputers and convergence acceleration techniques, turbulent solution CPU times on unstructured grids have been reduced to a number of hours. Unstructured grids also have the inherent ability to be decomposed into equal or nearly equal subsections. This quality translates into perfect or near perfect load balance allowing the efficient use of massively parallel supercomputers.

The Air Force SEEK EAGLE ACFD (Applied Computational Fluid Dynamics) project wants to provide the store separation engineer with accurate, reliable and efficient CFD tools. From a CFD developer's point of view, capturing the fluid physics and resulting aerodynamics accurately with quick turnaround time is the goal. For store integration and certification, obtaining accurate carriage loads in a timely manner is very important. If this is accomplished, then CFD has demonstrated one of its relative contributions. Trajectory generation/analysis, ejector modeling, etc. are separate technology areas which are best addressed by store certification experts.

Past demonstrative efforts have used several combinations of grid and flow solver techniques. Accurate predictions of store carriage loads on a generic wing/pylon/finned-store configuration[1-5] were presented in 1992. These results were mostly Euler calculations on a "simple" geometry. In 1996, a more complex aircraft/store configuration was studied, the F-16/generic finned-store[6-8]. However, questions about the accuracy of the wind-tunnel measurements were raised in that study. In addition, incorporating CFD tools into the certification process has been slowed by a lack of validations and demonstrations on "real" configurations.

The F/A-18C JDAM configuration was chosen for this study because both wind-tunnel measurements and flight-test data exist. For the flight test, both photogrametrics and telemetry were used to track the

---

* Aerospace Engineer, Computational Sciences Branch

flight path of the released JDAM. The wind-tunnel test used a six-percent scale F/A-18C model. Both a Captive Trajectory System (CTS) and a pylon mounted JDAM approach were used in the wind tunnel. The CTS and carriage wind-tunnel measurements correlated well with each other at only a few select conditions[9]. JDAM trajectories generated from these data were compared with flight-test values, and an inverse approach was used to determine the actual carriage loads which matched flight-test trajectories[9].

This document describes the JDAM aerodynamic loads and trajectory results obtained using the Air Force Research Laboratory (AFRL) *Cobalt*$_{60}$ flow solver and the Naval Air Warfare Center (NAWC) *NAVSEP* trajectory generator. Overviews of each method are provided in the following sections, and flowfield and trajectory results at two Mach numbers are given in the final sections.

Overview of *Cobalt*$_{60}$

Cobalt$_{60}$ is a parallel, implicit unstructured flow solver developed by the Computational Sciences Branch of the Air Force Research Laboratory[10]. Godunov's first-order accurate, exact Riemann method[11] is the foundation of *Cobalt*$_{60}$. Second-order spatial accuracy, second-order accurate implicit time stepping, viscous terms and turbulence models have been added to this procedure. *Cobalt*$_{60}$ uses a finite-volume, cell-centered approach. Arbitrary cell types in two or three dimensions may be used, and a single grid may be composed of a variety of cell types. Information on the calculation of inviscid and viscous fluxes and the dissipation in *Cobalt*$_{60}$ is reported in Strang[10]. Two one-equation turbulence models have been implemented in *Cobalt*$_{60}$, the Spalart-Allmaras[12] model and the Baldwin-Barth model[13].

The implicit algorithm in *Cobalt*$_{60}$ was implemented and demonstrated by Tomaro[14]. The implicit algorithm resulted in a 5-10 times speed up over the original explicit algorithm with only a ten-percent increase in memory. Inviscid flows were routinely obtained with CFL numbers of one million; however, turbulent flows severely limited the CFL number. A further modification to the original implicit algorithm, reported by Strang[10], removed the limitation for viscous flows, allowing CFL numbers of one million for most problems. This modified implicit algorithm resulted in a 7-10 times speed up in convergence over the original explicit code for viscous flows.

The development of the parallel version of *Cobalt*$_{60}$ was reported by Grismer[15]. Domain decomposition is the basis for the parallel code. Each processor operates on a subsection (zone) of the original grid. Information is passed between processors using the Message Passing Interface (MPI) library routines. *Cobalt*$_{60}$ has been implemented and tested on IBM SP2's, Cray T3E's and SGI Origin 2000's. The resulting speed up of *Cobalt*$_{60}$ demonstrated "superscalability" on large cache-based systems; i.e., the speed-up factor was greater than the number of processors used.

Cobalt$_{60}$ allows a variety of boundary conditions[16]. For these F/A-18C simulations, the farfield was imposed using a modified Riemann invariant method. The surfaces of the body were slip walls for an inviscid surface or adiabatic no-slip walls for a viscous surface. To account for flow through the engine, a source/sink pair was utilized. The engine face used a corrected mass flow sink boundary condition to enforce the mass flowing out the grid at this boundary surface. The engine exhaust was modeled with a source boundary condition to allow flow into the domain from this boundary surface.

Grid Resolution/Physics Study

Three separate grids were constructed to simulate the flowfield around the F/A-18C with stores. These three grids were used for a resolution study as well as a level of physics study. The equation set used in the simulation impacts the solution time as well as the aerodynamics. Therefore, it is important to know which level of physics is required for an engineering analysis. To that end, an inviscid solution, a stores-only viscous solution and a full viscous solution were calculated and compared. All three grids modeled the complete F/A-18C including the inlet duct to the engine face, the boundary layer diverter with flow through to the upper surface of the wing, the stair-stepped pylons, and the strakes on the JDAM including the notches.

The fully inviscid grid contained 3.15 million tetrahedral cells. *Cobalt*$_{60}$ required approximately 2.4 Gb of memory for this case. The grid was generated using Gridtool and VGRIDns[17], both programs developed by NASA Langley. The F/A-18C was essentially the first grid attempted with VGRIDns by the first author. The first step is to construct patches over the original PLOT3D surfaces. This step required approximately one week. Subsequently, some patches were further refined. The same surface patching was used as a basis for all three grids. The second step is to place sources to control grid spacing and clustering. This is an iterative step until the desired spacing is achieved. Two days were spent on this process. The third step is to triangulate the surface patches and project them to the original PLOT3D surfaces. This required one day. The final step is to generate the volume mesh; this step required approximately one hour on an SGI Octane workstation. Figure 1a displays the inviscid grid around the outboard pylon and JDAM. Notice that the notches in the strakes were modeled.

The second grid treated the surfaces of the JDAM and fuel tank as viscous surfaces. The rest of the aircraft was simulated with slip walls. This grid was generated using the inviscid surface patching but specifying the surfaces of the JDAM and fuel tank as viscous surfaces. The second grid contained 3.96 million tetrahedral cells with approximately 850,000 cells in the boundary layers requiring approximately 6.0 Gb of memory for this case. This modification to the grid required approximately one day. The generation of the volume grid again required one hour of CPU time. Figure 1b shows the viscous grid around the JDAM and the inviscid grid around the outboard pylon. Essentially, the same grid clustering was used.

The full viscous grid contained 6.62 million tetrahedral cells including approximately 4 million cells in the boundary layers. This grid was constructed by specifying all surface patches of the inviscid grid as now being viscous. For the full viscous case, *Cobalt*$_{60}$ required approximately 10.1 Gb of memory. If everything had proceeded smoothly, this step would have taken a one-day effort. However, the advancing front in VGRIDns actually kept growing "into" the body. After consulting with the VGRIDns experts at NASA Langley, it was determined the surface grid may have contained some folded triangles and that the clustering of negative volumes in the viscous layer were the causes (the negative volume cells are removed and then filled with the advancing front method). To remove these two problems, more sources were added and strengths modified during a trial and error process. This entire process required about a month of calendar time. The full viscous grid spacing around the JDAM and outboard pylon is shown in Figure 1c. Figures 2a and 2b show the viscous grid clustering at a fuselage station and a water-line of the aircraft, respectively.

Overview of *NAVSEP*

Store trajectories may be obtained when carriage loads and isolated store aerodynamics are provided to an independent six-degree-of-freedom, rigid-body motion solver. For this F/A-18C JDAM effort, AFRL obtained and used the NAWC *NAVSEP* trajectory generation program[18]. This code is used routinely by the Navy, and it requires minimal computer resources and user intervention requirements. *NAVSEP* is based on the AEDC trajectory generation system[19] embedded in its captive trajectory testing setup. The program integrates the standard conservation of linear and angular momentum equations for a rigid body experiencing aerodynamic and other body forces and moments.

The use of *NAVSEP* in this study was limited to JDAM trajectory generations based on *Cobalt*$_{60}$-derived aerodynamics (carriage and freestream), Navy-supplied ejector modeling and JDAM inertial properties. Table 1 summarizes the store property inputs required.

Weight	2059.44 lbs
Length	152.4 in
c.g. Location (x,y,z)	453.084, 134.28, 69.795 in
Forward Ejector Location	442.974 in
Forward Ejector Force (Peak)	4680 lbs
Aft Ejector Location	462.974 in
Aft Ejector Force (Peak)	4680 lbs
Ejector Stroke Lengths (2 Stages)	0.524, 6.015 in
Roll Moment of Inertia, Ixx	20.02 slug-ft^2
Pitch Moment of Inertia, Iyy	406.56 slug-ft^2
Yaw Moment of Inertia, Izz	406.59 slug-ft^2
Product of Inertia, Ixz(=Izx)	-0.68 slug-ft^2
Product of Inertia, Ixy(=Iyx)	0.86 slug-ft^2
Product of Inertia, Iyz(=Izy)	0 slug-ft^2
Roll Damping Coefficient, C_{lp}	-3/rad
Pitch Damping Coefficient, C_{mq}	-141/rad
Yaw Damping Coefficient, C_{nr}	-126/rad

Table 1: JDAM Properties Input to *NAVSEP*

In addition to the JDAM aerodynamics and above properties, information related to a decay function must be supplied to *NAVSEP*. This function varies with lateral and vertical distance of a store with respect to the carriage position such that the carriage loads dominate the effective aerodynamic forces and moments at and near the initial release point. Later, the loads decay to the freestream, isolated store aerodynamics. Typically the vertical separation distance is much larger than the lateral displacement, and when a store falls anywhere from 7 to 10 body diameters away, it is considered to be outside the carriage influence region.

Results

Two flight conditions were simulated on the three grids. The first test case was at Mach number M_∞ = 0.962 with α = 0.46° at an altitude of 6,332 ft. The second flight condition was an altitude of 10,832 ft with a Mach number M_∞ = 1.055 and α = -0.65°. The Spalart-Allmaras turbulence model was used in the viscous cases. For these simulations, the right side of the aircraft was modeled. The x-axis runs aft from the nose to the tail; the y-axis is positive out the right wing; and the z-axis is positive upward. Since the flight test tracked the JDAM on the left wing, there will be some sign changes required to match the CFD results, the wind-tunnel measurements and the flight-test data. The geometric reference quantities used to obtain the aerodynamic coefficients are presented in Table 2.

Reference Area	254.45 in^2
Moment Reference Length (x-axis)	18.0 in
Moment Reference Length (y-axis)	18.0 in
Moment Reference Length (z-axis)	18.0 in
Moment Reference Center (at JDAM c.g.)	453.084, 134.28, 69.795 in

Table 2: Geometric Reference Quantities for JDAM Aerodynamic Forces and Moments, Aircraft Reference Axes

Flowfield: M_∞ = 0.962

All three grids were used in the transonic simulations. Figures 3a-c show the convergence histories for axial force (F_x), side force (F_y) and normal force (F_z) for the various grids/physics requested. Each simulation was run 2,000 iterations, but the solutions are converged by 800 iterations. These forces are reported in the body-axis system of the entire aircraft.

In addition to grid clustering, Figures 1a-c show pressure contours on the JDAM. A high pressure region exists at the nose due to the stagnation point. There is another high pressure region at the beginning of the JDAM module; this JDAM module appears to have a sheet metal base that is attached only to the store itself. The JDAM module also includes the strakes. The high pressure region is due to the thickness of this sheet medal plate acting as a forward facing ramp, which was obviously modeled in the grids. The flow then expands as this ramp becomes parallel with the store surface again causing a lower pressure region. A shock aft of this position causes another pressure rise. Comparing Figure 1a with Figures 1b and 1c, the shock has clearly moved forward as is expected with the inclusion of viscous effects.

Table 3 compares the JDAM force and moment coefficients for this flight condition. Note that the moments were taken about an incorrect reference center location, with respect to the z-axis, which was corrected prior to the trajectory simulations. The coefficients are further referenced to the aircraft axis system discussed previously, and are not consistent with the JDAM body-axis definitions used for the wind-tunnel or flight-test data.

	Inviscid	Viscous Stores	Viscous
C_N	0.1408	0.1280	0.1122
C_A	0.6467	0.6921	0.7014
C_Y	-0.2992	-0.3136	-0.2843
C_m	-1.9807*	-2.1668*	-2.1697*
C_n	-2.2706*	-2.4630*	-2.4515*
C_l	0.1695*	0.1826*	0.1796*

*Incorrect reference location:
x_{cg} = 453.08, y_{cg} = 134.28, z_{cg} = 66.51 inches

Table 3: JDAM Right-Wing Carriage Loads for M_∞ = 0.962, *Cobalt$_{60}$* Aircraft Axis System

Note that the normal force has decreased with the addition of viscous forces. Axial force has been increased in the viscous simulations as expected. Side force varied slightly in the three different simulations. There are significant changes in the forces and moments between the inviscid simulation and the viscous simulations. However, the forces and moments vary slightly between the viscous stores simulation and the full viscous simulation. Therefore, to accurately predict the carriage loads for an engineering analysis, treating only the stores as viscous seems sufficient.

The inviscid case was simulated on 32 processors of an IBM SP2. The wall clock time was 4.90 hrs, the solution time per CPU was 4.87 hrs and the total CPU time was 155.84 hrs. The viscous stores grid was run on 36 processors of an IBM SP2. This solution required a wall clock time of 4.85 hrs, 4.72 hrs for each CPU and a total CPU time of 169.78 hrs. The viscous stores simulation had an average y^+ of 4.38. The full viscous case used 50 IBM SP2 processors. This simulation had an average y^+ of 3.65. The wall clock time required was 17.69 hrs. The total CPU time was 861.0 hrs with each CPU requiring 17.22 hrs. The above times are for converged solutions at 800 iterations.

Figure 5a shows pressure contours at a water line of 135 in, a position above the F/A-18C wing. Notable flow features include the expansion around the front half of the canopy, a shock wave near the middle of the canopy, and shock waves aft of the boundary layer diverter. Since the flow has accelerated to supersonic speeds over the upper fuselage, a shock wave exists in front of the vertical tails due to their presence. The interesting shock is the normal shock between the trailing edges of the vertical tails. Figure 5b shows the complex flowfield interactions below the wing at a water line station of 72 in which intersects the JDAM and fuel tank. The expansions due to the JDAM module and the shock wave on the module can clearly be seen. A low pressure region between the aft ends of the fuel tank and the JDAM gives rise to the inboard pointing side force. Aft of the two stores, there are a series of intersecting oblique shocks which the released JDAM must pass through.

Trajectory: $M_\infty = 0.962$

The JDAM carriage loads from the viscous *Cobalt$_{60}$* simulation (see Table 3) were transformed to the correct store body-axis reference system. This system is aligned with the JDAM body axis which is pitched down 3° with respect to the aircraft axis and is centered at the JDAM c.g. location. A further modification was required to determine forces and moments for the left-wing configuration. The final carriage results, listed in Table 4, are consistent with the flight-test configuration where the x-axis points forward along the JDAM centerline, the y-axis points inboard, and the z-axis points downward. Note that the normal force is positive in the negative z-direction, and the axial force is positive in the negative x-direction. The pitching moment coefficient from *Cobalt$_{60}$* of C_m = -2.2854 matches the carriage and CTS wind-tunnel measurements of C_m = -2.3, (see Cenko[9] for all flight-test data and wind-tunnel measurements). The *Cobalt$_{60}$* yawing moment coefficient result of C_n = -2.4403 falls in the range of the carriage C_n = -2.80 and CTS measurement of C_n = -1.55. *Cobalt$_{60}$* calculated a side force coefficient of C_Y = 0.2844 which slightly underpredicts the flight-test and wind-tunnel values of C_Y = 0.31. The normal force coefficients were measured as C_N = 0.15 for the flight test and C_N = 0.105 for the wind tunnel which are slightly larger than the *Cobalt$_{60}$* value of C_N = 0.0753. Overall, the carriage loads from *Cobalt$_{60}$* matched very well with the flight-test and wind-tunnel data.

C_N	0.0753
C_A	0.7063
C_Y	0.2844
C_m	-2.2854
C_n	-2.4403
C_l	0.0177

Table 4: JDAM Body-Axis Carriage Loads for M_∞ = 0.962

A series of 5-alpha and 5-beta sweeps for the isolated JDAM were also conducted with *Cobalt$_{60}$*, and the numerical results were placed in a data table for *NAVSEP*. All the required JDAM properties from Table 1 and other input parameters such as altitude and Mach number were also supplied. Trajectory results using decay functions based on 7-10 diameters exhibited large discrepancies when compared to the flight-test data. Therefore, the decay function was selected to eliminate the carriage loads effects after the JDAM had fallen about 1-1.5 diameters away from the pylon. This modification suggests that the aerodynamic loads on the JDAM in the transition region between carriage and the freestream are changing rapidly as strong flow gradients exist in the early stages of release. A grid-based aerodynamic data matrix or a fully-integrated, moving-mesh CFD capability may be required to obtain more accurate trajectories.

Predicted JDAM trajectory parameters are compared to the flight-test telemetry and photogrametric data in Figures 7a-c. Note that the axial and vertical displacements are underpredicted, whereas the pitch and yaw angles are overpredicted. A roll reversal occurs during the ejection sequence in flight, as shown by the data in Figure 7c, therefore the roll angle and roll rate are not well predicted by the simple ejector model used in *NAVSEP*.

The predicted pitch rate overshoots the maximum flight-test value at about 0.14 sec (see Figure 7c), and then recovers by 0.25 sec. The predicted yaw rate recovers more rapidly than the flight-test values which indicate a nearly flat rate between 0.15-0.25 sec.

Figure 7d illustrates the time history of the miss distance, or clearance, between the JDAM and any portion of the F/A-18C aircraft including the pylons and fuel tank. Due to the reversed roll attitude seen in the prediction, the near-zero miss distance between 0.1-0.13 sec can be attributed to the JDAM's upper outboard fin coming very close to the bottom aft end of the pylon.

Flowfield: M_∞ = 1.055

Simulations on the three grids were completed for the supersonic case. The convergence histories for axial force (F_x), side force (F_y) and normal force (F_z) for the various grids/physics requested are shown in Figures 4a-c. Each simulation was run 2,000 iterations, but the solutions were again converged by 800 iterations. These forces are reported in the body-axis system of the entire aircraft.

The JDAM carriage force and moment comparisons for the three grid systems are presented in Table 5. Note that the moments were again taken about an incorrect reference location (which was corrected prior to the trajectory simulations), and the reference axis was for the aircraft. The same changes in magnitudes of the forces were seen for this case as for the M_∞ = 0.962 flight condition. Again, there are significant changes in the forces and moments between the inviscid simulation and the viscous simulations but slight changes between the viscous stores simulation and the full viscous simulation. For an engineering analysis, only the stores need to be treated as viscous surfaces.

The inviscid case was simulated on 32 processors of an IBM SP2. The wall clock time was 4.95 hrs, the solution time per CPU was 4.92 hrs and the total CPU time was 157.57 hrs. The viscous stores grid required 4.84 hrs of wall clock time, 4.70 hrs on each CPU and 169.34 hrs of total CPU time. The solution was run on 36 processors of an IBM SP2. The viscous stores simulation had an average y^+ of 4.12. The full viscous case used 32 IBM SP2 processors. This simulation had an average y^+ of 3.46. The wall clock required time was 26.87 hrs. The total CPU time was 840.0 hrs with each CPU requiring 26.27 hrs. The above times are for converged solution at 800 iterations.

Figure 6a shows pressure contours at a water line of 135 in, a position above the F/A-18C wing. Shock waves exist in front of the nose and in front of the canopy, and a well defined shock is positioned in front of the wing due to blockage effects. As in the M_∞ = 0.962 case, shocks sit after the boundary layer diverter and before the vertical tails. A relatively strong shock sits at the aft end of the aircraft. Figure 6b shows the complex flowfield interactions below the wing at a water line station of 72 in which intersects the JDAM and fuel tank. As in the M_∞ = 0.962 case, expansion and shock waves on the JDAM module can clearly be seen. A low-pressure region between the aft ends of the fuel tank and the JDAM causes the inboard-pointing side force. Aft of the two stores, there is a another series of intersecting oblique shocks which the released JDAM passes through. These oblique shocks are further aft than those of the M_∞ = 0.962 case.

	Inviscid	Viscous Stores	Viscous
C_N	0.0840	0.0347	0.0224
C_A	0.6236	0.6826	0.6873
C_Y	-0.2728	-0.2825	-0.2572
C_m	-1.9362*	-2.0835*	-2.0651*
C_n	-2.0465*	-2.2403*	-2.1909*
C_l	0.1908*	0.4346*	0.2019*

*Incorrect reference location:
x_{cg} = 453.08, y_{cg} = 134.28, z_{cg} = 66.51 inches

Table 5: JDAM Right-Wing Carriage Loads for M_∞ = 1.055, *Cobalt$_{60}$* Aircraft Axis System

Trajectory: M_∞ = 1.055

The JDAM carriage loads from *the fully viscous case* (see Table 5) were transformed to the JDAM body-axis system described previously. A further modification was performed to provide loads consistent with the flight-tested left-wing configuration. The final carriage results are listed in Table 6. The x-axis points forward along the JDAM centerline, the y-axis points inboard, and the z-axis points downward. The pitching moment coefficient for the carriage and CTS wind-tunnel measurements of C_m = -2.15, (see Cenko[9] for all flight-test data and wind-tunnel measurements) was slightly overpredicted by the *Cobalt$_{60}$* value of C_m = -2.2335. The *Cobalt$_{60}$* yawing moment coefficient result of C_n = -2.2111 falls in the range of the carriage C_n = -2.60 and CTS measurement of C_n = -2.15. *Cobalt$_{60}$* predicted a side force coefficient of C_Y = 0.2572 which closely approximated the flight-test and wind-tunnel values of C_Y = 0.25. The normal force coefficients were measured as C_N = 0.05 for the flight test and C_N = 0.03 for the wind tunnel which are slightly larger than the *Cobalt$_{60}$* value of C_N = -0.0136. Overall, the carriage loads from *Cobalt$_{60}$* matched very well with the flight-test and wind-tunnel data.

A series of 8-alpha and 5-beta sweeps for the isolated JDAM were also conducted with *Cobalt$_{60}$*, and the numerical results were placed in a data table for *NAVSEP*. Similar to the previous Mach number case, trajectory predictions using decay functions based on 7-10 diameters exhibited large discrepancies when compared to the flight-test data. Again, the decay function was selected to eliminate the carriage loads effects after the JDAM had fallen about 1-1.5 diameters away from the pylon. Strong flow gradients exist in the early stages of release, and the transition region between carriage and freestream aerodynamics is difficult to predict. Grid-based studies, integrated moving-mesh CFD or other influence-based means are required to obtain more accurate aerodynamics in the near-pylon region.

C_N	-0.0136
C_A	0.6876
C_Y	0.2572
C_m	-2.2335
C_n	-2.2111
C_l	0.0129

Table 6: JDAM Body-Axis Carriage Loads for M_∞ = 1.055

Resulting JDAM trajectory parameters are compared to the flight-test telemetry and photogrametric data in Figures 8a-c. Note that the c.g. displacements are well predicted, whereas the pitch and yaw angles are overpredicted as in the previous Mach number case. Again, a roll reversal occurs during the ejection sequence in flight (see Figure 8c), therefore the roll angle and roll rate are not well predicted by the simple ejector model used in *NAVSEP*.

The predicted pitch rate overshoots the maximum flight-test value at about 0.15 sec (see Figure 8c), and then recovers after 0.25 sec. The predicted yaw rate recovers more rapidly than the flight-test values, and by 0.25 sec, this rate is increasing in the opposite direction. A sudden increase in predicted yaw angle, as shown in Figure 8b, results from the yaw rate reversal.

Figure 8d illustrates the time history of the miss distance between the JDAM and F/A-18C aircraft, including the pylons and fuel tank. Due to the predicted roll attitude which is opposite to the flight-test data, the near-zero miss distance between 0.1-0.14 sec can be attributed to the JDAM's upper outboard fin coming in very close proximity to the bottom aft end of the pylon. Despite the poor prediction of roll angle at about 0.2 sec, the predicted miss distance is in agreement with the telemetry data.

Conclusions

Store carriage loads for a complex air vehicle system were obtained accurately and rapidly using viscous unstructured-grid CFD methodology. The *Cobalt$_{60}$* flow solver developed by the Air Force Research Laboratory was able to resolve relevant compressible, viscous flow features which dictate the aerodynamic loading. The parallel processing feature in *Cobalt$_{60}$* further enables rapid turnaround time for a single solution, such that in a week's time, many carriage configurations may be simulated during a parametric investigation.

Store separation trajectories were generated with the Naval Air Warfare Center's *NAVSEP* code, a separate rigid-body, six-degree-of-freedom motion solver. All CFD-based aerodynamics, as well as store inertial properties, were simply tabulated and input. The resulting trajectories correlated well with the flight-test data in the earliest stages of release, and then departed from the data when the carriage effects were considered to be diminished. Sources of such discrepancies were likely due to simple ejector modeling characteristics and general difficulties in determining suitable aerodynamics in regions of rapidly changing mutual interference between the store and parent vehicle.

Acknowledgments

The authors would like to thank J. Garriz and S. Pirzadeh for their help with VGRIDns. All the simulations in this paper were run using the IBM SP2 located at the ASC/MSRC, Wright-Patterson AFB, OH.

References

1. Lijewski, L. and Suhs, N., "Chimera-Eagle Store Separation," AIAA 92-4569, August 1992.

2. Meakin, R. L., "Computations of the Unsteady Flow About a Generic Wing/Pylon/Finned-Store Configuration," AIAA 92-4568, August 1992.

3. Newman, J. C. and Baysal, O., "Transonic Solutions of a Wing/Pylon/Finned-Store Using Hybrid Domain Decomposition," AIAA 92-4571, August 1992.

4. Parikh, P., Pirzadeh, S., and Frink, N. T., "Unstructured Grid Solutions to a Wing/Pylon/Store Configuration Using VGRID3D/USM3D," AIAA 92-4572, August 1992.

5. Jordan, J. K., "Computational Investigation of Predicted Store Loads in Mutual Interference Flow Fields," AIAA 92-4570, August 1992.

6. Madson, M. and Talbot, M., "F-16/Generic Carriage Load Predictions at Transonic Mach Numbers using TRANAIR," AIAA 96-2454, June 1996.

7. Cline, D., Riner, W., Jolly, B., and Lawrence, W., "Calculation of Generic Store Separations from an F-16 Aircraft," AIAA 96-2455, June 1996.

8. Kern, S. B. and Bruner, C. W. S., "External Carriage Analysis of a Generic Finned-Store on the F-16 Using USM3D," AIAA 96-2456, June 1996.

9. Cenko, A., "F-18/JDAM CFD Challenge Wind Tunnel Flight Test Results," AIAA 99-0120, January 1999.

10. Strang, W. Z., Tomaro, R. F., and Grismer, M. J., "The Defining Methods of *Cobalt*$_{60}$: A Parallel, Implicit, Unstructured Euler/Navier-Stokes Flow Solver," AIAA 99-0786, January 1999.

11. Godunov, S. K., "A Difference Scheme for Numerical Computation of Discontinuous Solution of Hydrodynamic Equations," *Sbornik Mathematics,* vol 47, p. 271-306, 1959.

12. Spalart, P. R. and Allmaras, S. R., "A One-Equation Turbulence Model for Aerodynamic Flows," AIAA 92-0439, January 1992.

13. Baldwin, B. S. and Barth, T. J., "A One-Equation Turbulence Transport Model for High Reynolds Number Wall-Bounded Flows," NASA TM 102847, August 1990.

14. Tomaro, R. F, Strang, W. Z., and Sankar. L. N., "An Implicit Algorithm for Solving Time Dependent Flows on Unstructured Grids," AIAA 97-0333, January 1997.

15. Grismer, M. J., Strang, W. Z., Tomaro, R. F., and Witzeman, F. C., "Cobalt: A Parallel, Implicit, Unstructured Euler/Navier-Stokes Solver," *Advances in Engineering Software,* Vol 29, No. 3-6, pp. 365-373, Apr-Jul 1998.

16. Strang, W.Z., "Parallel *Cobalt*$_{60}$ User's Manual," AFRL/VAAC, WPAFB, OH, August 1998.

17. Pirzadeh, S., "Three-Dimensional Unstructured Viscous Grids by the Advancing-Layers Method," *AIAA Journal*, Vol. 34, No. 1, January 1996, p. 43-49.

18. Cenko, A., private communication, January 1998.

19. Carmen Jr., J. B., Hill Jr., D. W., and Christopher, J. P., "Store Separation Testing Techniques at the Arnold Engineering Development Center, Vol II, Description of Captive Trajectory Store Separation Testing in the Aerodynamic Wind-Tunnel (4T)," AEDC-TR-79-1, June 1980.

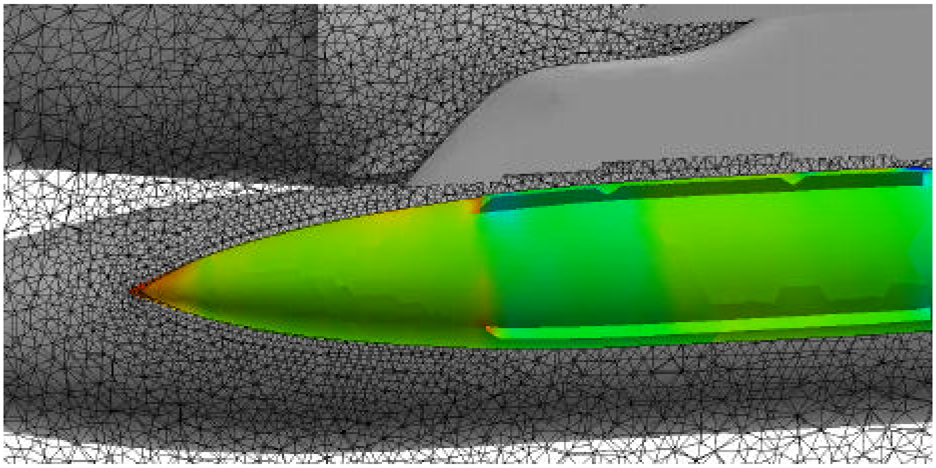

Figure 1a: Inviscid Grid Near the JDAM and the Outboard Pylon

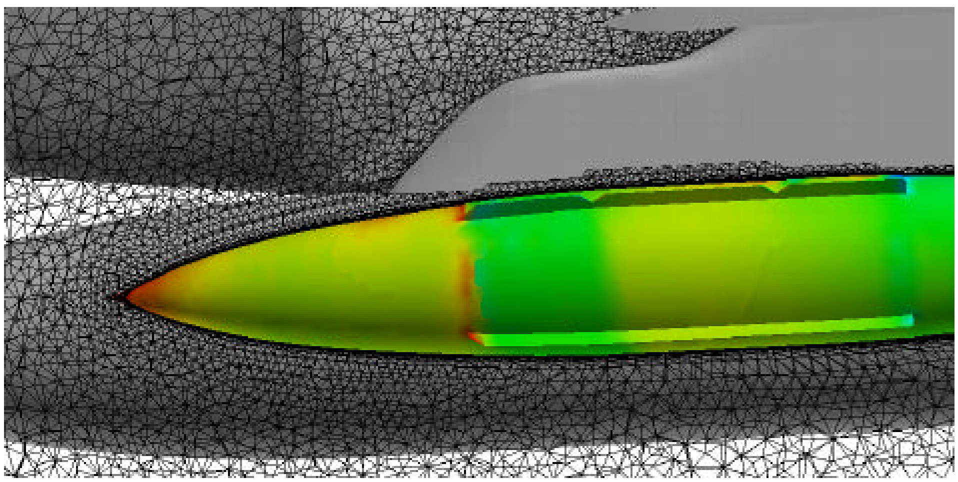

Figure 1b: Viscous Stores Grid Near the JDAM and the Outboard Pylon

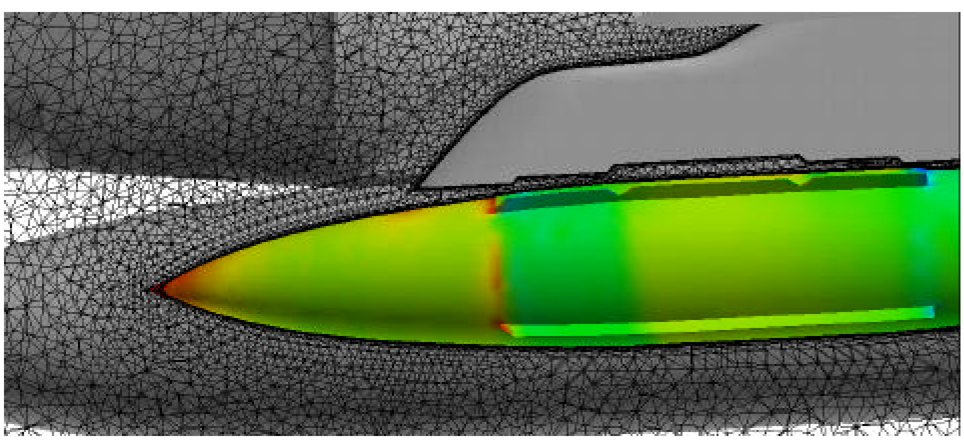

Figure 1c: Viscous Grid Near the JDAM and the Outboard Pylon

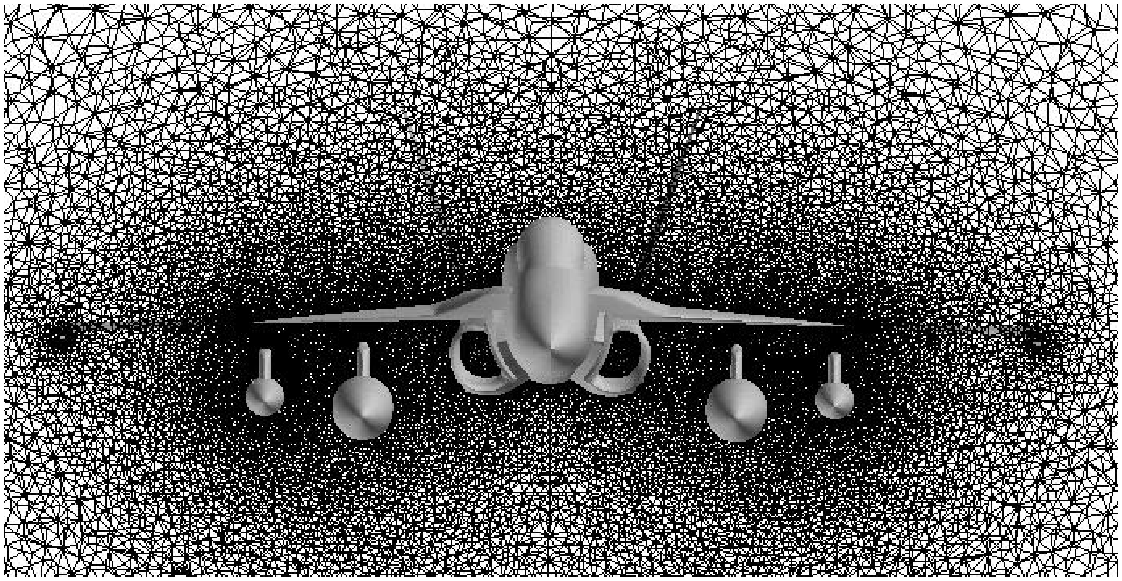

Figure 2a: Viscous Grid Clustering at a Fuselage Station through the JDAM

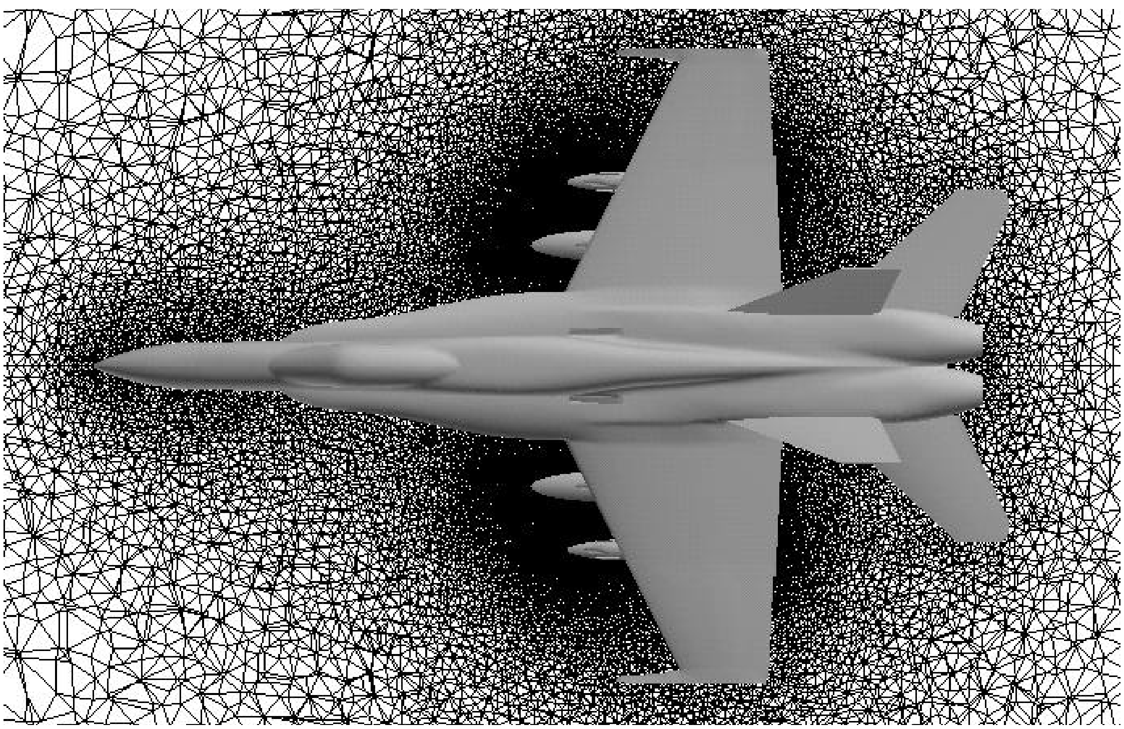

Figure 2b: Viscous Grid Clustering at a Water Line through the JDAM

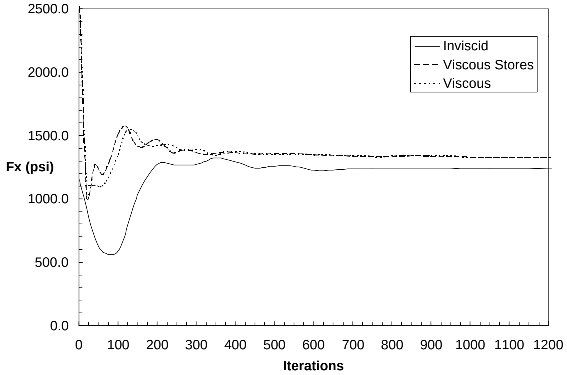

Figure 3a: Convergence History of Axial Force on the JDAM, M_∞ = 0.962

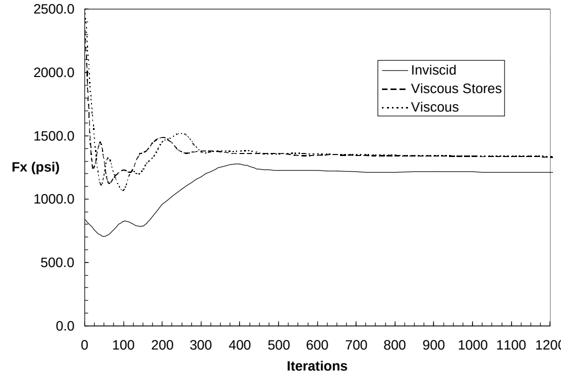

Figure 4a: Convergence History of Axial Force on the JDAM, M_∞ = 1.055

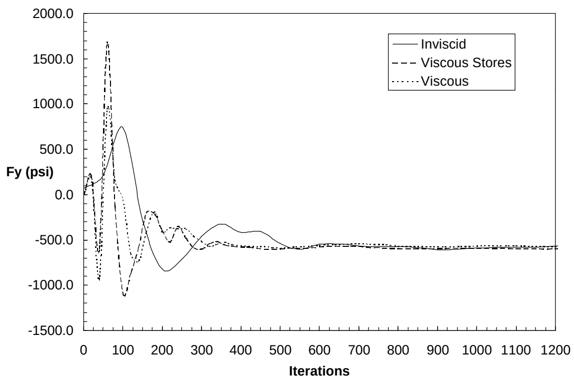

Figure 3b: Convergence History of Side Force on the JDAM, M_∞ = 0.962

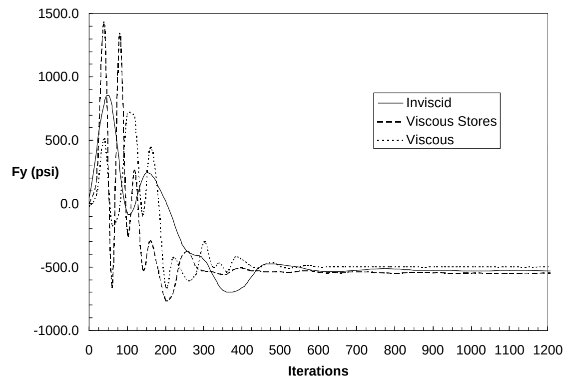

Figure 4b: Convergence History of Side Force on the JDAM, M_∞ = 1.055

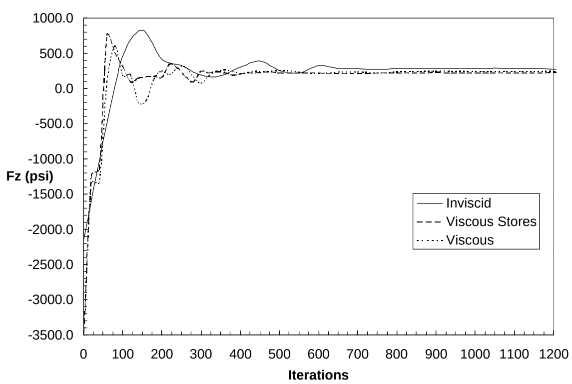

Figure 3c: Convergence History of Normal Force on the JDAM, M_∞ = 0.962

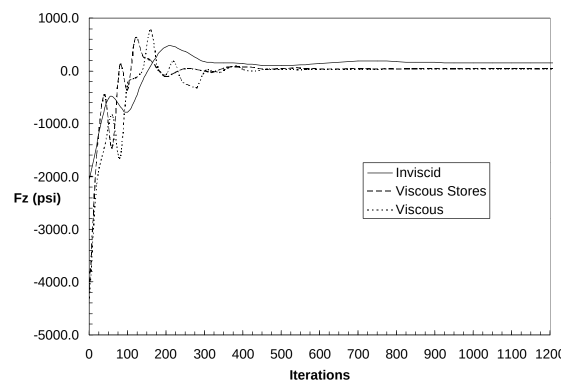

Figure 4c: Convergence History of Normal Force on the JDAM, M_∞ = 1.055

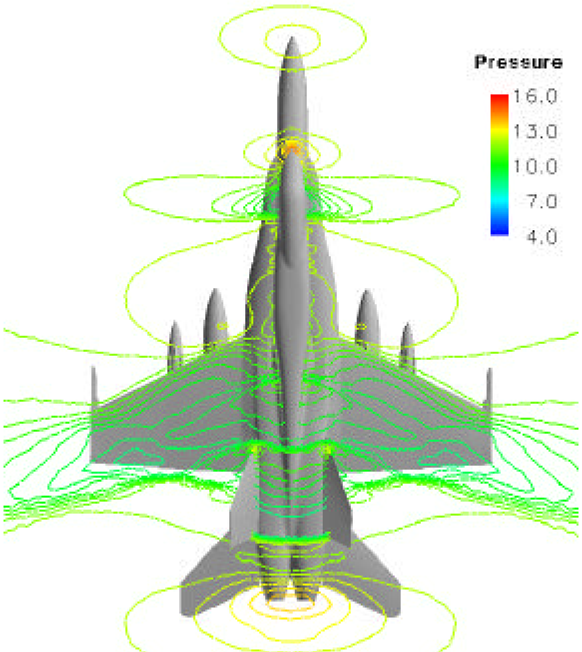

Figure 5a: Pressure Contours at Water Line = 135 in, M_∞ = 0.962

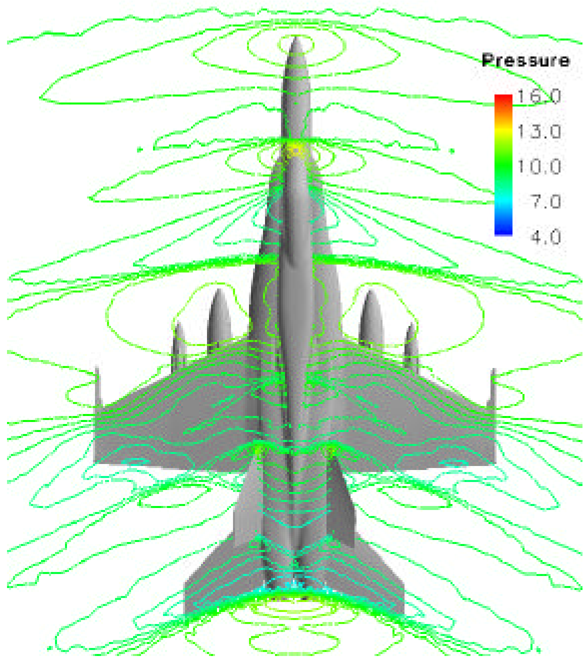

Figure 6a: Pressure Contours at Water Line = 135 in, M_∞ = 1.055

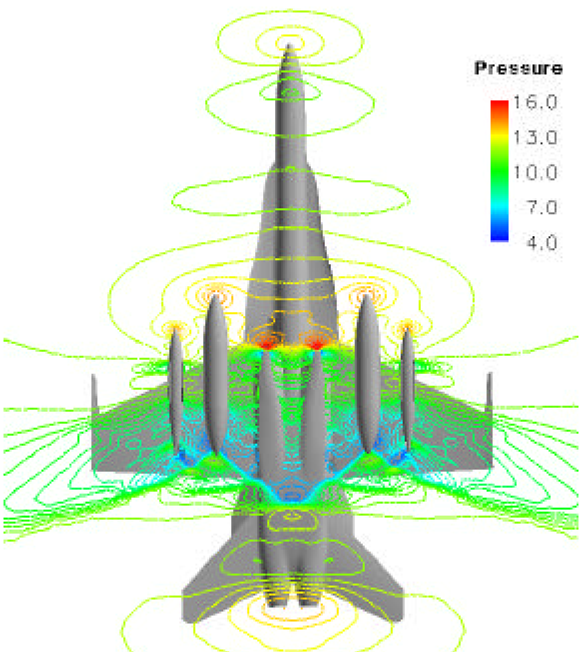

Figure 5b: Pressure Contours at Water Line = 72 in, M_∞ = 0.962

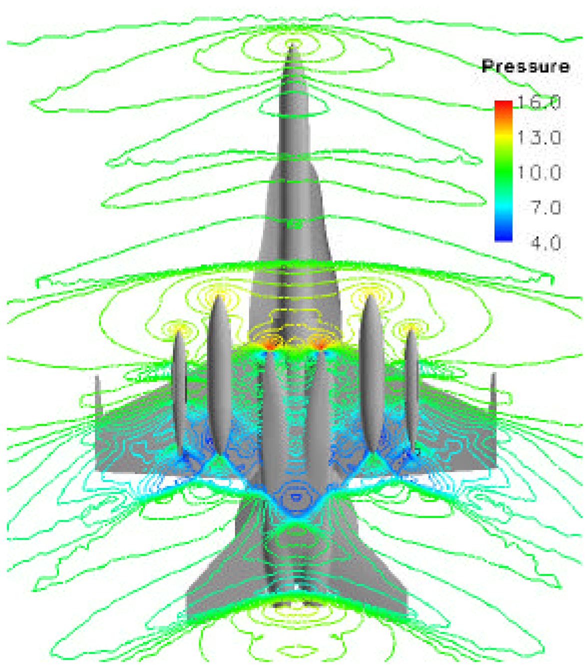

Figure 6b: Pressure Contours at Water Line = 72 in, M_∞ = 1.055

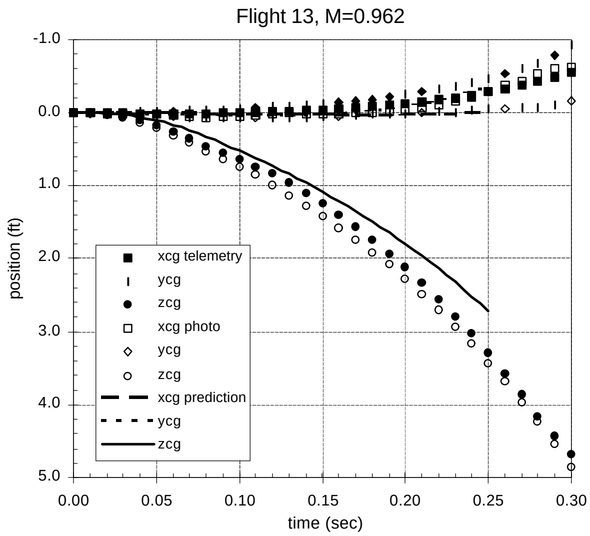

Figure 7a: JDAM c.g. Locations, M$_\infty$=0.962

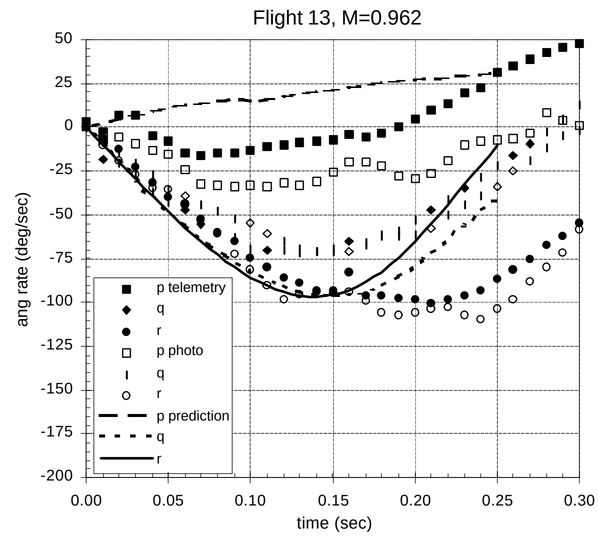

Figure 7c: JDAM Angular Rates, M$_\infty$=0.962

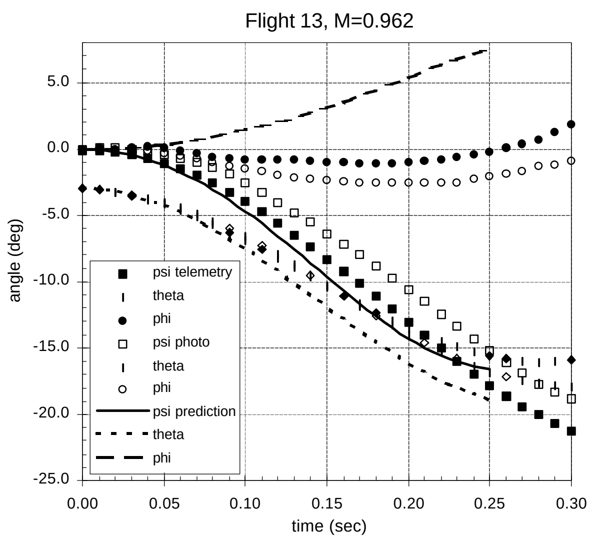

Figure 7b: JDAM Attitudes, M$_\infty$=0.962

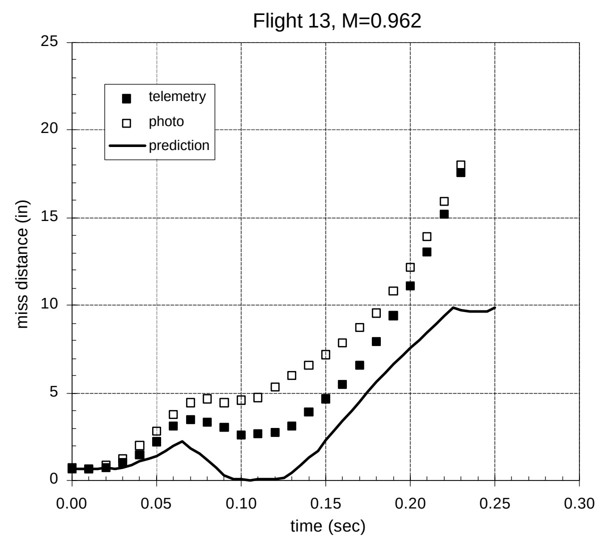

Figure 7d: JDAM Miss Distance, M$_\infty$=0.962

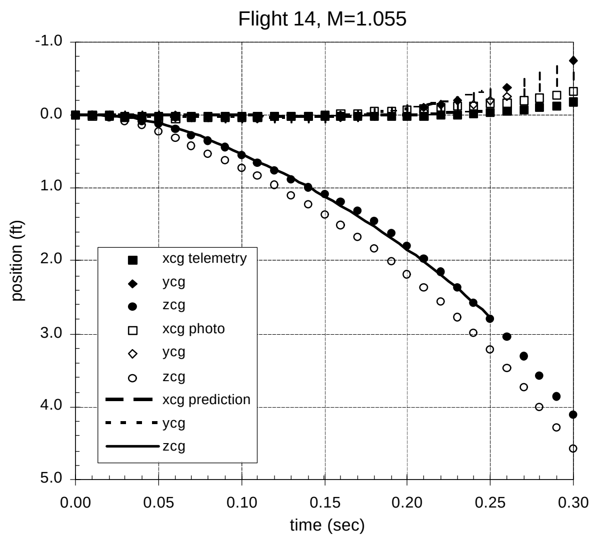

Figure 8a: JDAM c.g. Locations, M$_\infty$=1.055

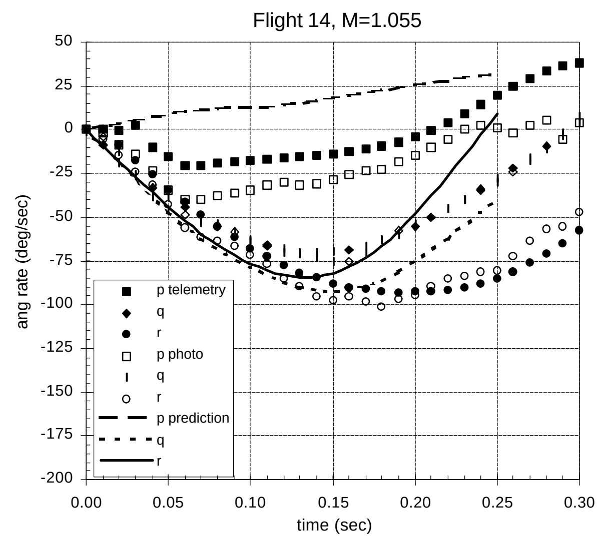

Figure 8c: JDAM Angular Rates, M$_\infty$=1.055

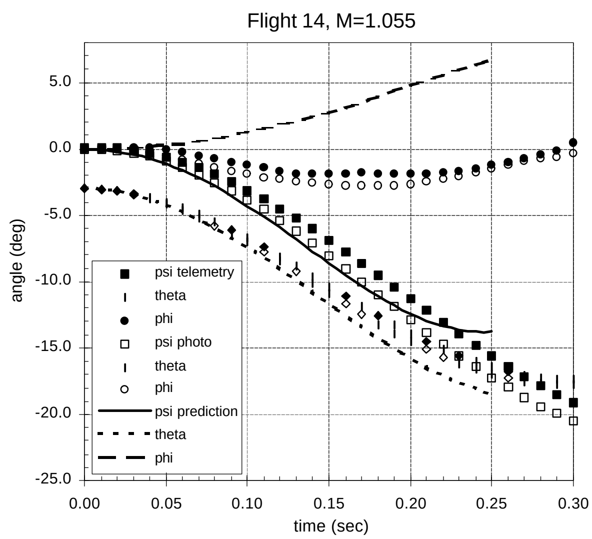

Figure 8b: JDAM Attitudes, M$_\infty$=1.055

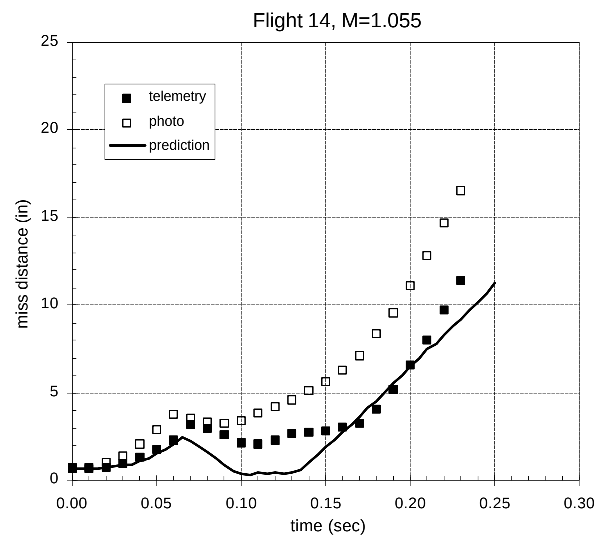

Figure 8d: JDAM Miss Distance, M$_\infty$=1.055